https://doi.org/10.1016/j.envpol.2019.03.113

Characterizing Spatiotemporal Dynamics of Anthropogenic Heat Fluxes: A 20–year case study in the Beijing–Tianjin–Hebei region of China

Shanshan Chen[a, b], Deyong Hu[b,*], Man Sing Wong[c], Huazhong Ren[a], Shisong Cao[b], Chen Yu[b], Hung Chak Ho[d]

a Institute of Remote Sensing and Geographic Information System, Peking University, Beijing 100871, China

b College of Resource Environment and Tourism, Capital Normal University, Beijing 100048, China

c Department of Land Surveying and Geo-Informatics, The Hong Kong Polytechnic University, Hong Kong

d Department of Urban Planning and Design, The Hong Kong University, Hong Kong

* Corresponding author. College of Resource Environment and Tourism, Capital Normal University, 100048, Beijing, China

E-mail address: deyonghu@163.com (D.Y. Hu).

Abstract: Rapid urbanization has resulted in a great amount of anthropogenic heat emissions, which is closely related to economic growth, human health, and micro-climate. The lack of long-term anthropogenic heat emissions estimation data is of great concern to climate and urban fluxes research. This study estimated annual average anthropogenic heat fluxes in Beijing-Tianjin-Hebei region of China between 1995 and 2015 based on the multi-sources of remote sensing images and ancillary data. The anthropogenic heat emissions from different sources (including industries, buildings, traffics and human metabolism) were also estimated to analyze the composition of anthropogenic heat fluxes. And the spatiotemporal dynamics of the long-term AHF with high spatial resolution (500-m) were estimated by the Refined Anthropogenic Heat Flux model and then analyzed using trend analysis and standard deviation ellipse analysis. The results showed that values in the region increased significantly from 0.15 $W \cdot m^{-2}$ in 1995 to 1.46 $W \cdot m^{-2}$ in 2015. The heat emissions from industries, traffics, buildings and human metabolism accounted for 64.1%, 17.0%, 15.5% and 3.4% of the total anthropogenic heat emissions, respectively. Industrial energy consumption was the dominant contributor to the anthropogenic heat emissions in the region. During this period, the industrial heat emissions presented unstable variation, but overall showed a growing trend. Heat emissions from the buildings had increased linearly. The spatial distribution

was extended with an increasing tendency of the difference between the maximum and the minimum, and it was generally dominated by the "northeast-southwest" directional pattern. Based on the aforementioned results, the spatiotemporal distribution patterns and trends of anthropogenic heat fluxes could provide vital support on management decision in city planning and environmental monitoring.

Keywords: Anthropogenic heat; Human activities; Spatiotemporal dynamics; Nighttime light data; Thermal environment monitoring; Mitigation

1 Introduction

Anthropogenic heat is the heat released to the atmosphere as a result of human activities. Sources of anthropogenic heat include industrial activities, heating and cooling of buildings, human metabolism, and vehicle exhausts (American Meteorological Society, 2018). Urbanization and economic development in China has been accelerating over the past 30 years which draws increasing attentions of scientific community (Bai et al., 2014). The amount of energy consumed has considerably increased with population growth and economic growth, and almost all the energy consumption for human activities can eventually transform into anthropogenic heat fluxes (Taha, 1997, Feng et al., 2014). In the statistics of International Energy Agency (IEA), China's energy consumption increased from 1,045 million tonnes oil equivalent (Mtoe) (in 1995) to 2,976 Mtoe (in 2015) (IEA 2016). The increasing human activities release more and more anthropogenic heat to the atmosphere with the rapid urbanization. Urbanization and anthropogenic heat are crossly-interacted, e.g. growth of population, increased energy consumption for economy, and expansion of built-up areas would lead to a growth of anthropogenic heat emissions (Feng et al., 2012; Iamarino et al., 2012; Wong et al., 2015). At the same time, the anthropogenic heat released into the atmosphere have important implications on urbanization by affecting city micro-climate, human health, and air quality (Block et al., 2004; Xie et al., 2016; Nie et al., 2017). As such, anthropogenic heat is a representative urban energy forcing, and is playing an important role as input into weather/climate models. Anthropogenic heat flux (AHF) is defined as a measurement of the heat released into the environment by human activities, i.e., anthropogenic heat emissions generated per unit time and

area (Taha, 1997). Hence, accurate and reliable estimation of AHF is a need for meteorological modeling, heat-related public health study, and thus characterizing of spatiotemporal dynamics of AHF is crucial for understanding both the impacts and mechanisms of AHF, and its interactions with urbanization.

Previous studies have estimated AHF at different scales, such as block scale (Kłysik, 1996; Zhao et al., 2011; Sun et al., 2018), city scale (Hamilton et al., 2009; Hu et al., 2012; Lee et al., 2015), regional scale (Lindberg et al., 2013; Lu et al., 2016; Koralegedara et al., 2016) and global scale (Flanner, 2009; Allen et al., 2011; Yang et al., 2017). For the AHF estimation at regional scale or global scale, the top-down inventory-based methods are the most useful and frequently used method (Sailor et al., 2004; Sailor et al., 2011). Energy consumption data used in this method always collected at administrative units. Thus, to estimate AHF at a finer scale, aggregated spatial information is used, such as population density, pollutant emissions and nighttime light (NTL) data. For example, Lindberg and Grimmond (2013) estimated the AHF in Europe between 1995 and 2015 based on population density data. Dong et al. (2017) used a population dataset adjusted by NTL data to estimate global AHF with a high spatial resolution of 30 arc-seconds. In addition, in order to simplify the estimation method, regression analysis was always adopted (Chen et al., 2012; Lee et al., 2014; Koralegedara et al., 2016).

The Refined Anthropogenic Heat Flux (RAHF) model is another method to simulate the annual average gridded AHF based on a new generation Suomi-NPP VIIRS NTL data and a top-down inventory-based method (Chen and Hu, 2017). Compared with existing global AHF datasets of Flanner (2009) and the large scale urban energy consumption model (LUCY) developed by Allen et al. (2011), the AHF results of RAHF model have significant merits in the representation of spatial details. The results of this model can depict the spatial details of AHF in administrative units. NTL data is one of the spatial proxy data of socioeconomic statistics and energy consumption data (Li et al., 2012; Li et al., 2013; Coscieme et al., 2014; Zhou et al., 2015). It can detect low intensity light emitted by the residents and has a unique superiority in the monitoring of human activities at nighttime. In this paper, in order to estimate and model the long-term AHF, DMSP/OLS NTL data were adopted and used in RAHF model since the new generation NTL data were only available since 2012. However, there are some discrepancies between DMSP/OLS NTL data and Suomi-NPP

VIIRS NTL data due to different satellite platforms (Elvidge et al., 2013; Shi et al., 2014). Consequently, to obtain continuous and comparable long-term annual average AHF, we need to minimize the discontinuity effect between years caused by different platforms/sensors.

Despite the numerous estimation of AHF in different cities, there is a lack of research on AHF in Beijing-Tianjin-Hebei (BTH) region at high spatial resolution, and covers a study period for a decade (Hu et al., 2012; Wang et al., 2016; Sun et al., 2018). Some historical studies and research projects have focused on the influence of anthropogenic heat on the urban environment and development (Ichinose et al., 1999; Sailor et al., 2004; Narumi et al., 2009; Chrysoulakis et al., 2018). The impact of anthropogenic heat emission comes from the continuous evolution of human activities in both time and space. Therefore, the analysis of urban environment and development also requires the evolution process of anthropogenic heat from two dimensions of "time" and "space". BTH region is the capital economic region in China. Under the political importance of BTH region, the spatial-temporal distribution of AHF in this region can provide auxiliary information for decision-making of city planning and environmental monitoring. However, existing literature and study in this topic of BTH region is still sparse and rudimentary (Nie et al., 2014). Therefore, it is essential to conduct a comprehensive study by investigating the long-term spatiotemporal dynamics of AHF in this region.

The main objectives of this study are (1) to calculate the anthropogenic heat emissions during the past two decades based on prefectural-level statistics and to analyze the composition of anthropogenic heat emissions in BTH region; (2) to estimate the long-term AHF using RAHF model and multi-source remote sensing data, and then parameterize pixel-based AHF between 1995 and 2015; (3) to evaluate spatiotemporal dynamics of AHF in BTH region using trend analysis and standard deviation ellipse analysis for providing holistic information related to urban heat island study.

2 Study area and Data

2.1 Study area

The Beijing-Tianjin-Hebei region (BTH region) was selected as the study area, due to a long

winter period, thus lots of energy such as coal and natural gas were consumed during winters. Meanwhile, energy consumption used for heating in winters and cooling in summers account for about 19% of energy demand in China (Wang, 2002). The BTH region is an economic development center in the northern China, includes Beijing municipality, Tianjin municipality and eleven prefecture-level cities of Hebei Province (Fig. 1(a)).

In 2015, the resident population (RP) of BTH region was about 110 million people, and the regional GDP was about 6.94 trillion yuan (Fig. 1(b), (c)). The total energy consumption was about 445.08 million tons of standard coal. The anthropogenic heat is mainly from the heat discharges of automobile exhaust emissions, the energy consumption of industrial production, and the various energy consumptions of buildings (e.g., winter heating and summer air-conditioning/refrigeration).

2.2 Data

The socioeconomic data and energy consumption data for energy-consumption inventory approach were collected from the China Statistical Yearbooks, China Energy Statistical Yearbooks and corresponding City Statistical Yearbooks, including GDP of the three industries (GDP_{I}, GDP_{II}, GDP_{III}), RP, acreage, and the amount of civil automobile at provincial and prefectural level and so on. Considering the availability of data in BTH region and the energy-consumption inventory, we sorted out the index needed and estimated the missing individual data by the ratio of the same type of index using linear regression. In order to facilitate comparison and calculation, the physical quantity of energy was converted into energy standard consumption according to each energy type and the corresponding conversion factor (Council et al., 1999).

MOD13A1 Level-3 16-day 500-m NDVI products from April 2000 to October 2015 were acquired from LAADS web. These products have been used to monitor the Earth's terrestrial photosynthetic vegetation activity in many other studies (Anderson et al., 2005; Tomar et al., 2014; Hajiloo et al., 2018). The quality control was performed based on the QC subset of NDVI images. The annual composites nighttime light (NTL) data were used to detect spatiotemporal dynamics of AHF in this study. A summary and the source of data used in this study are illustrated in supplementary materials (S1).

3 Methodology

3.1 Estimating prefectural-level heat emissions from different sources

According to the emission sources of anthropogenic heat, anthropogenic heat emissions are divided into four major components: the energy consumption from industry (labeled as E_I), buildings (E_B), transportation (E_V), and human metabolism (E_M). Total anthropogenic emission (E_F) is equal to the sum of the four parts:

$$E_F = E_I + E_B + E_V + E_M \quad (1)$$

$$E_I^i = \frac{GDP_{II}^i + GDP_{III}^i}{\sum_{i=1}^{n}(GDP_{II}^i + GDP_{III}^i)} \times E_I \times C \quad (2)$$

$$E_B^i = \left[\frac{GDP_{III}^i}{\sum_{i=1}^{n}\left(GDP_{III}^i\right)} \times E_{Bc} + \frac{RP_i}{\sum_{i=1}^{n}(RP_i)} \times E_{Br}\right] \times C \quad (3)$$

$$E_V^i = d \times FE \times \rho \times NHC \times V_i \quad (4)$$

$$E_M^i = (P_1 t_1 + P_2 t_2) \times RP_i \times 3600 \times 365 \quad (5)$$

E_I^i is the industrial energy consumption of prefectural-level city i, the prefectural-level heat emission from industries is distributed based on the proportion of the second GDP (GDP_{II}^i) and third industrial GDP (GDP_{III}^i) of each city. RP represents the resident population. C is standard coal heat, equal to 29,306 $kJ \cdot kg^{-1}$; E_{Bc}, E_{Br} are the energy consumption from residential and commercial buildings respectively. d is the annual average driving distance per vehicle (unit: km); FE is the combustion efficiency (unit: $L \cdot km^{-1}$); ρ is the combustion density (unit: $kg \cdot L^{-1}$); NHC is the net heat combustion (unit: $kJ \cdot g^{-1}$). V is the amount of civil automobile. P_1, P_2 are the metabolic rate of sleeping and active state respectively. t_1, t_2 are hours of sleeping (7:00~23:00) and active time (23:00~7:00) respectively.

3.2 Parameterizing pixel-based AHF from nighttime light data

RAHF model was used to obtain pixel-based AHF which can clearly demonstrate the spatial distribution of AHF. The details of RAHF model building can be found in supplementary materials (S3) (Chen and Hu, 2017). Using the strong correlation between annual mean AHF and mean human

settlement index (HSI), it introduces an effective approach for linking incomplete statistical socio-economy data with NTL data (Lu et al., 2008).

For a long-time series AHF parameterization, the difference between DMSP/OLS NTL data and Suomi-NPP VIIRS NTL data should be considered. Owing to the limitation of the OLS itself, there are always saturated in the center of the city where the light intensity is high. Saturation of NTL data limits the range difference in actual light intensity within the saturated region, which in turn affects the accuracy of AHF estimation. It is, therefore, worthwhile to diminish the saturation values so that the spatiotemporal dynamics of AHF can be modeled accurately. The Vegetation Adjusted NTL Urban Index (VANUI) proposed by Zhang et al (2013) was used to minimize the discontinuity effect between years and reduce the saturation effect of NTL data considering the highly negative correlation between vegetation and human activities. The formula is as follows:

$$\mathrm{VANUI} = (1 - \mathrm{NDVI}) \times \mathrm{NTL}_{nor} \quad (6)$$

which NDVI is the value between 0 to 1 of MOD13A1 NDVI product, and NTL_{nor} is the normalized NTL data.

Three main procedures were undertaken to derive time-series annual average AHF using the NTL data: firstly, estimating prefectural-level heat emissions based on statistical data, and the results were used as samples for RAHF modeling; secondly, inter-calibration the NTL data using the VANUI; and thirdly, estimating pixel-based AHF using the inter-calibrated NTL data and RAHF model.

3.3 Evaluation of spatiotemporal dynamics of AHF

3.3.1 Trend analysis of change in AHF

Trend analysis is commonly used in temporal dynamic analysis to explore inter-annual variation characteristics. A linear slope analysis was used to evaluate the spatiotemporal dynamics of AHF between 1995 and 2015, which has been suggested as effective means to detect the trend in time-series data (He et al., 2012; Peng et al., 2016). The formula of the slope is listed below:

$$\mathrm{slope} = \frac{n*\sum_{i=1}^{n} i*AHF_i - (\sum_{i=1}^{n} i)(\sum_{i=1}^{n} AHF_i)}{n*\sum_{i=1}^{n} i^2 - (\sum_{i=1}^{n} i)^2} \quad (7)$$

where AHF_i is the pixel-based AHF. n is the time span, and i is the time unit. A positive slope was

192 indicated that there was an increasing change trend in AHF. If the slope was near zero, the category
193 was a stable type. A negative slope indicated an obvious decreasing trend in AHF.
194 Then, the Natural Break method was applied to classify the spatial distribution of AHF
195 differencing map. The map was classified into five grades: no-obvious-growth (<0.30 $W \cdot m^{-2}$), low-
196 growth (0.30-1.13 $W \cdot m^{-2}$), moderate-growth (1.13-2.41 $W \cdot m^{-2}$), relatively-high-growth (2.41-4.14
197 $W \cdot m^{-2}$) and high-growth (4.14-5.65 $W \cdot m^{-2}$). The Natural Break method was selected and aimed to
198 investigate statistical variations in different areas, and it provided the smallest variances between
199 categories, without the influence of artificial factors (Brewer et al., 2015; Shi et al., 2016).

200 *3.3.2 Standard deviation ellipse analysis on the spatial pattern of AHF*

201 Standard Deviation Ellipse (SDE) is one of the classical methods for analyzing directional
202 features of spatial distribution. It can express the main distribution direction of a set of points and
203 the degree of dispersion in every direction; these two features are usually used to describe the overall
204 characteristics of a geospatial distribution (Peng et al., 2016). In this study, SDE of pixel-based AHF
205 results was utilized for characterizing the spatial pattern of AHF in BTH region. Some parameters
206 are used to describe the characteristics of SDE, including deflection angle, radius of primary axis
207 and auxiliary axis. The radius of primary and auxiliary axis reflects the concentrated density of the
208 overall elements of the spatial pattern, and the declination angle reflects the dominant direction of
209 the pattern. The formulas for these parameters are presented in the studies of David (1999) and
210 Lauren et al. (2010).

211 **4 Results**

212 *4.1 Heat emissions from different sources*

213 Anthropogenic heat emissions from different sources in the cities of BTH region from 1995 to
214 2015 are shown in Fig. 2. It shows the anthropogenic heat emissions vary over time. The heat
215 emissions from the industry were varied during the period between 1995 and 2015, but overall, the
216 cities except Beijing municipality showed a growing trend. Industrial heat emissions were affected
217 by the land use planning and the urban economic orientation. The heat emissions from industry in
218 Beijing grew rapidly between 1995 and 2000, but it had gradually decreased since 2000, which was

closely related to the economic orientation of Beijing municipality in BTH region. Beijing issued a policy of industrial relocation to protect the environment and improve air quality in year 2006. The results show that Tianjin municipality, Tangshan and Shijiazhuang cities are the main sources of industrial heat emissions in BTH region. More details about the change of the heat emissions from different sources were shown in supplementary materials (S2).

The anthropogenic heat emissions in 2015 were taken as an example to analyze the composition of anthropogenic heat emissions in BTH region. The results are shown in Fig. 3(a). The composition of anthropogenic heat emissions in other years were shown in supplementary materials (S2). From the overall perspective of BTH region, the heat emissions were mostly coming from industry, followed by the traffic and building heat emissions, and finally the human metabolic heat emissions. The heat emissions from industry, transportation, buildings and human metabolism accounted for 64.1%, 17.0%, 15.5% and 3.4% of the total anthropogenic heat emissions, respectively. The anthropogenic heat emissions in Hebei Province and Tianjin municipality were mainly from industry, and the anthropogenic heat emissions in Beijing municipality were mainly from buildings. Specifically, the anthropogenic heat emissions in Hebei Province, Beijing municipality, and Tianjin municipality were 9.96×10^{18} J, 1.68×10^{18} J, and 2.38×10^{18} J respectively.

The heat emissions from industry, buildings, transportation and human metabolism were summed up in order to obtain the total amount of anthropogenic heat emissions of the cities/municipalities in BTH region, as shown in Fig. 3(b). The total anthropogenic heat emission in BTH region increased steadily during this period, from 3.78×10^{18} J in 1995 to 1.4×10^{19} J in 2015. The results show that the anthropogenic heat emissions in Tianjin municipality and the cities of Hebei Province showed an overall growth trend, while for the anthropogenic heat emissions in Beijing municipality, except for the rapid growth in 1995-2000, its growth rate had gradually decreased since 2000. The change of anthropogenic heat emission is largely influenced by the development policy of the city and the development of technology to improve energy consumption efficiency.

4.2 Time-series AHF parameterization results

The spatial and temporal distribution of AHF in BTH region between 1995 and 2015 were

modeled using the method described in Section 3.2. The statistical regression relationships between the average HSI and the AHF of the districts and counties of Beijing and Tianjin municipalities from 1995 to 2015 are shown in supplementary materials (S4). RAHF model is a mature method to estimate AHF in BTH region (Chen and Hu, 2017). It is based on the official statistics, and the estimation accuracy of RAHF model has been verified in two aspects. One is for the prefectural-scale AHF estimation modelling. The other one is for the grid-scale AHF results. Therefore, the long-term spatiotemporal analysis of AHF in this study is based on the belief that the AHF results estimated by the RAHF model are credible. The comparison between RAHF results and other AHF products is shown in supplementary materials (S5).

The pixel-based AHF results at 500-m resolution of BTH region in 1995, 2000, 2005, 2010 and 2015 were shown in Fig. 4. It can be seen that the AHF was gradually increasing and the high value range of AHF was also increasing over the past two decades. The areas with high AHF values were situated in city centers and the spatial extents of AHF was also spread over the past two decades with an increasing tendency of the difference between the maximum and the minimum. In order to quantitatively analyze the changes, the mean, maximum and standard deviations of AHF were calculated, and more details are provided in supplementary materials (S6).

4.3 Spatial dynamics of AHF between 1995 and 2015

Fig. 5 plots the spatial distribution and areal percentage of five grades of AHF growth in BTH region from 1995 to 2015. During the past two decades, the AHF growth rate shows a decreasing trend from urban areas to suburbs. The high-growth category of AHF growth was concentrated in each city center of BTH region, especially in airports, central business districts and industrial areas. These places are also the regions of high AHF value at each time node (Fig. 4). The growth of AHF was concentrated in 50.13% of the total area of BTH region, with no-obvious-growth, low-growth, moderate-growth, relatively-high-growth, and high-growth accounting for 47.59%, 1.51%, 0.54%, 0.26%, and 0.24% of the total area, respectively (Fig. 5(b)).

Fig. 5(c) illustrates the areal percentage of each AHF type in Beijing, Tianjin and Hebei. The no-obvious-growth type was concentrated in suburban and mountainous area, accounting for 60.89%, 63.52% and 82.33% of each area of Beijing, Tianjin and Hebei respectively. Of the total

area of Beijing, the low, medium and relatively-high types account for 20.45%, 9.82%, and 5.26%, respectively. The growth pattern of Tianjin is similar to that of Beijing. But, it should be pointed out that the high-growth grade was mainly located in Tianjin, covering 5.28% of its total area. In addition, Hebei was dominated by no-obvious-growth type (>80%). The AHF growth of the cities in Hebei Province is relatively slow. In summary, the spatiotemporal variations of AHF were mainly identified in Beijing and Tianjin municipalities, with no-obvious variations of AHF found in the cities of Hebei Province.

The distribution of mass center and motion trajectory of AHF in BTH region are shown in the lower right corner of Fig. 6. From 1995 to 2015, the mass center was located between Beijing and Tianjin municipalities. The motion trajectory was gradually shifted to the southeast from the south of Beijing municipality, and then shifted to the northeast since 2010. It indicates that the AHF in the southeast increased rapidly in the early stage and later in the northeast, but overall was shifted to eastward, which means that the AHF in the east of BTH region increased rapidly during this period. In addition, the magnitude of the mass center movement during 2000 to 2010 is significantly greater than that during the other time period. The change of AHF has obvious directionality during 2000 to 2010, while the change of AHF was multidirectional in other periods. The relevant parameters of the standard deviation ellipse of each year are shown in supplementary materials (S7).

5 Discussion

5.1 Implications of long-term AHF results for environmental application

Many past studies have already studied the effects of single-period AHF on urban heat island (UHI), air pollution, shallow groundwater temperatures and urban climate (Narumi et al., 2009; Nie et al., 2014; Boehme et al., 2015; Du et al., 2016; Yang et al., 2016; Benz et al., 2018; Adelia et al., 2019). AHF may influence the form and intensity of urban heat island by modifying the urban boundary layer structure through increased turbulence (Chow et al., 2014). The distribution of AHF in time and space is determining the local and overall contribution to the UHI (Kato et al., 2005). Current micrometeorological models (including urban canyons), which assume certain levels of homogeneity and wind phenomena in the planetary boundary layer (PBL), might not be applicable in tropical and high-dense cities. The long-term AHF results enable UHI research to identify critical

grid cells in simulations and could be applied for better accuracy (Boehme et al., 2015). AHF is considered as an important component of the urban representation in numeric weather prediction models and should be carefully accounted for when considering the urban surface energy balance. Long-time AHF spatial distribution results can provide evidence of the significance of AHF in urban environment and suggestions for improvement of urban module in numeric weather prediction models and to detect its effects on air quality.

The rapid increase of urbanization in China means an expansion of the built-up area, an increase in the population and a growth of the economic demand. The urbanization in BTH region between 1995 and 2015 was described in supplementary materials (S8). Anthropogenic heat is one of the products of urbanization. It is the heat released into the earth system in the form of external energy, which affects climate change, human health, urban water resources and air quality, and have an important impact on urban development. Conversely, continued urbanization associated with increasing energy demanding accelerates the switch to modern fuels, the rise in appliance and vehicle use, and demand for construction materials (International Energy Agency, 2017). The accelerating urbanization and the increasing frequency of human activities also influence anthropogenic heat emissions. Understanding the leading causes of the increase of anthropogenic heat emission during urbanization is helpful to propose solutions for AHF mitigation and design administrative functions for policy makers.

Theoretically, the growth of population, economy and built-up area inevitably lead to more anthropogenic heat. There is a positive correlation between them. But in fact, the results show that there is no absolute positive relationship between AHF and economic level, built-up area except for the relationship between population and AHF. Higher economic levels do not correspond to more anthropogenic heat emissions (Fig. 1, Table S4). It is related to the new low-energy, low-emission industries that have been conducted in some cities. These new energy-saving measures effectively control the generation of anthropogenic heat and also create economic value for cities. Beijing is a typical example with high economic level, but the AHF is not the highest in BTH region (Fig. 3(b)).

The built-up area of Beijing increased from 477 km^2 in 1995 to 1401 km^2 in 2015. Among this, the built-up area increased greatly from 2000 to 2005, but the increase of anthropogenic heat emissions during the corresponding period was not the most intense (Fig. 3(b)). In contrast, the

growth of built-up area in 1995-2000 was slower, while the increase of anthropogenic heat emissions during the corresponding period was most dramatic. It can be seen that although the increase of built-up area has a certain promoting effect on anthropogenic heat emissions, it is not the main cause of the change of anthropogenic heat emissions, however the human activities occurring within the city are the main causes of the increase of anthropogenic heat emissions.

The spatial distribution is mainly consistent with the expansion direction of built-up areas. This finding is consistent with previous studies (Lu et al., 2016; Dong et al., 2017). Another finding from the long-term AHF results is that anthropogenic heat emissions are mainly affected by the population size and the intensity of human activities such as industrial production, residential life and transportation within the city. Starting from the urbanization that has a positive effect on anthropogenic heat emissions, it can effectively control anthropogenic heat emissions from the aspects of improving efficiency of industrial energy use and household appliance, advocating the concept of energy conservation and emission reduction, developing renewable energy and clean energy technologies.

5.2 Limitations and prospects

Several studies investigated the characteristics of AHF at various spatiotemporal scales (Flanner, 2009; Allen et al., 2011; Yang et al., 2017). It is found that the AHF varies with the spatial scales, and the value increases with the increasing spatial resolution (Zhou et al., 2012; Chen and Hu, 2017). To ensure the continuity and comparability between the spatiotemporal AHF results, the VAHUI index was used to eliminate the difference of the spatial resolution and detection ability between the nighttime light data from different sensors. However, the AHF in 2015 is much larger than the rest of the year. The main reason for this growth is the increase in energy consumption and heat emissions from various sources, but for pixel-based AHF results, another reason is the significant improvement in spatial resolution, which has increased from approximately 1000m to 500m.

Long-term AHF spatial distribution results can provide support for application research in many local areas, there are also some studies on regional spatiotemporal characteristics of AHF around the world at present (Iamarino et al., 2012; Nie et al., 2014; Koralegedara et al., 2016; Benz et al., 2018). However, due to the differences of regional data statistics and estimation methods, the

results are not absolutely comparable, which increases the difficulty of large-scale environmental research. Therefore, in the future, it is necessary to consider the construction of comparability methods for AHF results, such the local climate zone (LZC) established in UHI for easy comparison (Stewart et al., 2012). And in studying the impact of AHI on UHI, it is meaningful to obtain comparable AHI products for UHI research.

6 Conclusions

To have thoroughly understanding of variation of anthropogenic heat is essential for city planning, environmental monitoring and climatic research. The 500-m resolution grid-scale AHF over BTH region in the year 1995, 2000, 2005, 2010 and 2015 were estimated based on RAHF model. And the spatiotemporal distribution characteristics of AHF in BTH region were analyzed for the first time. The following conclusions can be drawn:

(1) The anthropogenic heat emissions continued to increase in most areas of BTH region from 1995 to 2015, and the AHF increased significantly from 0.15 $W \cdot m^{-2}$ in 1995 to 1.46 $W \cdot m^{-2}$ in 2015.

(2) During this period, the industrial heat emissions presented unstable variation, but overall showed a growing trend. Heat emissions from the buildings had increased linearly.

(3) Industrial energy consumption was identified as the dominant contributor. In 2015, the heat emissions from industries, traffics, buildings and human metabolism accounted for 64.1%, 17.0%, 15.5% and 3.4% of the total anthropogenic heat emissions, respectively.

(4) Spatial variability of AHF was obvious in BTH region. The spatial distribution was generally dominated by the "northeast-southwest" directional pattern. The areas with high AHF values were identified as city centers and the spatial extend of high AHF value was also expanding over the past two decades.

Overall, this study has studied and showed the detailed characteristics of changes of AHF in BTH region in recent twenty years, and developed an approach to estimate long-term AHF at high spatial resolution for a large metropolitan area. These long-term aggregated AHF data can further be used for other study e.g. micro-climatic study, environmental monitoring project, and the data

389 can help to pinpoint the spatial areas of Urban Heat Island in the region.

390 Acknowledgements

391 This research was supported by the grant National Natural Science Foundation of China (No.
392 41671339). Dr. Man Sing Wong specially thanks the funding support from Early Career Scheme
393 from the Research Grants Council of Hong Kong (No. 25201614); the Research Institute for
394 Sustainable Urban Development (No. 1-BBWD), and grants from the Hong Kong Polytechnic
395 University (No. 1-ZE24 & 1-ZVN6).

396 Appendix A. Supplementary data

397 Supplementary data related to this article can be found at XXX

398 References

399 Adeia A.S., Yuan C., Liu L., Shan R.Q., 2019. Effects of urban morphology on anthropogenic heat dispe
400 rsion in tropical high-density residential areas. Energy Build. 186, 368–383. https://doi.org/10.1016/j.e
401 nbuild.2019.01.026

402 American Meteorological Society, 2018. Anthropogenic heat. Glossary of Meteorology. Available online at
403 http://glossary.ametsoc.org/wiki/Anthropogenic_heat (Accessed 2 Sep 2018).

404 Allen, L., Lindberg, F., Grimmond, C.S.B., 2011. Global to city scale urban anthropogenic heat flux: model and
405 variability. Int. J. Climatol. 31, 1990–2005. https://doi.org/10.1002/joc.2210

406 Anderson L.O., Shimabukuro Y.E., Defries R.S., Morton D., 2005. Assessment of deforestation in near real time
407 over the Brazilian Amazon using multitemporal fraction images derived from Terra MODIS. IEEE Geosci.
408 Remote Sens. Lett. 2(3), 315–318. https://doi.org/10.1109/LGRS.2005.850364

409 Bai X., Shi P., Liu Y., 2014. Society: Realizing China's urban dream. Nat. 509(7499), 158–60. https://doi.
410 org/10.1038/509158a

411 Benz S. A., Peter B., Philipp B., Hamamoto H., Arimoto H., Taniguchi M., 2018. Comparing anthropoge
412 nic heat input and heat accumulation in the subsurface of Osaka, Japan. Sci. Total Environ. 643, 11
413 27–1136. https://doi.org/10.1016/j.scitotenv.2018.06.253
414 Block A., Keuler K., Schaller E., 2004. Impacts of anthropogenic heat on regional climate patterns. Geophys. Res.
415 Lett. 31(12), 179206. https://doi.org/10.1029/2004GL019852
416 Boehme P., Berger M., Massier T., 2015. Estimating the building based energy consumption as an anthropogenic
417 contribution to urban heat islands. Sust. Cities Soc. 19, 373–384. https://doi.org/10.1016/j.scs.2015.05.006
418 Brewer C.A., Pickle L., 2015. Evaluation of Methods for Classifying Epidemiological Data on Choropleth Maps in
419 Series. Ann. Assoc. Am. Geogr. 92(4), 662–681. https://doi.org/10.1111/1467-8306.00310
420 Chen S.S., Hu D.Y., 2017. Parameterizing Anthropogenic Heat Flux with an Energy-Consumption Inventory and
421 Multi-Source Remote Sensing Data. Remote Sens. 9(11), 1165. https://doi.org/10.3390/rs9111165
422 Chen, B., Shi, G., 2012. Estimation of the Distribution of Global Anthropogenic Heat Flux. Atmos. Oceanic Sci.
423 Lett. 5, 108–112. https://doi.org/10.1080/16742834.2012.11446974
424 Chow W.T.L., Salamanca F., Georgescu M., Mahalov A., Milne J.M., Ruddell B.L., 2014. A multi-method
425 and multi-scale approach for estimating city-wide anthropogenic heat fluxes. Atmos. Environ. 99, 6
426 4–76. https://doi.org/10.1016/j.atmosenv.2014.09.053
427 Chrysoulakis N., Grimmond S., Feigenwinter C., Lindberg, F., Gastellu-Etchegorry J.P., Marconcini M., Mitraka Z.,
428 Stagakis S., Crawford B., Olofson F., Landier L., Morrison W., Parlow E., 2018. Urban energy exchanges
429 monitoring from space. Sci. Rep. 8(1), 11498. https://doi.org/11498. 10.1038/s41598-018-29873-x
430 Coscieme, L., Pulselli, F.M., Bastianoni, S., Elvidge, C.D., Anderson, S., Sutton, P.C., 2014. A thermodynamic
431 geography: night-time satellite imagery as a proxy measure of emergy. Ambio. 43, 969.
432 https://doi.org/10.1007/s13280-013-0468-5

433 Dong Y., Varquez A.C.G., Kanda M., 2017. Global anthropogenic heat flux database with high spatial resolution.
434 Atmos. Environ. 150, 276–294. https://doi.org/10.1016/j.atmosenv.2016.11.040
435 Du H.Y., Wang D.D., Wang Y.Y., Zhao X.L., Qin F., Jiang H., Cai Y.L., 2016. Influences of land cover
436 types, meteorological conditions, anthropogenic heat and urban area on surface urban heat island in
437 the Yangtze River Delta Urban Agglomeration. Sci. Total Environ. 571, 461–470. https://doi.org/10.1
438 016/j.scitotenv.2016.07.012
439 Elvidge C.D., Baugh K.E., Zhizhin M., Hsu F.C., 2013. Why VIIRS data are superior to DMSP for mapping
440 nighttime lights. Proc. Asia-Pac. Adv. Network 35, 62–69. https://doi.org/10.7125/APAN.35.7
441 Feng J.M., Wang Y.L., Ma Z.G., Liu Y.H., 2012. Simulating the Regional Impacts of Urbanization and A
442 nthropogenic Heat Release on Climate across China. J. Clim. 25(20), 7187–7203. https://doi.org/10.11
443 75/JCLI-D-11-00333.1
444 Feng J.M., Wang J., Yan Z.W., 2014. Impact of Anthropogenic Heat Release on Regional Climate in Three Vast
445 Urban Agglomerations in China. Adv. Atmos. Sci. 31(2), 363–373. https://doi.org/10.1007/s00376-013-3041-
446 z
447 Flanner M.G., 2009. Integrating anthropogenic heat flux with global climate models. Geophys. Res. Lett. 36, 270–
448 271. https://doi.org/10.1029/2008GL036465
449 Hajiloo F., Hamzeh S., Gheysari M., 2018. Impact assessment of meteorological and environmental parameters on
450 PM2.5 concentrations using remote sensing data and GWR analysis (case study of Tehran). Environ. Sci. Pollut.
451 Res. 8, 1–15. https://doi.org/10.1007/s11356-018-1277-y
452 Hamilton I.G., Davies M., Steadman P., Stone A., Ridley I., Evans S., 2009. The significance of the anthropogenic
453 heat emissions of London's buildings: A comparison against captured shortwave solar radiation. Build. Environ.
454 44(4), 807–817. http://dx.doi.org/10.1016/j.buildenv.2008.05.024

He C.Y., Ma Q., Li T., Yang Y., Liu Z.F., 2012. Spatiotemporal dynamics of electric power consumption in Chinese Mainland from 1995 to 2008 modeled using DMSP/OLS stable nighttime lights data. J. Geog. Sci. 22(1), 125–136. http://dx.doi.org/10.1007/s11442-012-0916-3

Hu D., Yang L., Zhou J., Deng L., 2012. Estimation of urban energy heat flux and anthropogenic heat discharge using aster image and meteorological data: case study in Beijing metropolitan area. J. Appl. Remote Sens. 6(1), 063559. https://doi.org/10.1117/1.JRS.6.063559

Iamarino M., Beevers S., Grimmond C.S.B., 2012. High-resolution (space, time) anthropogenic heat emissions: London 1970–2025. Int. J. Climatol. 32, 1754–1767. https://doi.org/10.1002/joc.2390

International Energy Agency, 2016. World Energy Outlook 2016. http://www.worldenergyoutlook.org/ (Accessed 2 Sep 2018).

International Energy Agency, 2017. World Energy Outlook 2017. http://www.iea.org/media/weowebsite/2017/Chap1_WEO2017.pdf. (Accessed 27 July 2018).

Kato S., Yamaguchi Y., 2005. Analysis of urban heat-island effect using ASTER and ETM+ Data: Separation of anthropogenic heat discharge and natural heat radiation from sensible heat flux. Remote Sens. Environ. 99(1-2), 44–54. https://doi.org/10.1016/j.rse.2005.04.026

Kłysik K., 1996. Spatial and seasonal distribution of anthropogenic heat emissions in Lodz, Poland. Atmos. Environ. 30(20), 3397–3404. https://doi.org/10.1016/1352-2310(96)00043-X

Koralegedara S.B., Lin C.Y., Sheng Y.F., Kuo C.H., 2016. Estimation of anthropogenic heat emissions in urban Taiwan and their spatial patterns. Environ. Pollut. 215, 84–95. https://doi.org/10.1016/j.envpol.2016.04.055

Lauren M.S., Mark V.J., 2010. Handbook of Applied Spatial Analysis: Software Tool, Methods and Applications. Springer, Berlin.

Lee S.H., Kim S.T., 2015. Estimation of anthropogenic heat emission over South Korea using a statistical regression

method. Asia-Pac. J. Atmos. Sci. 51(2), 157–166. https://doi.org/10.1007/s13143-015-0065-6

Lee S.H., Mckeen S.A., Sailor D.J., 2014. A regression approach for estimation of anthropogenic heat flu x based on a bottom-up air pollutant emission database. Atmos. Environ. 95(1), 629–633. https://doi.org/10.1016/j.atmosenv.2014.07.009

Li X., Xu H., Chen X., Li C., 2013. Potential of NPP-VIIRS Nighttime Light Imagery for Modeling the Regional Economy of China. Remote Sens. 5, 3057–3081. https://doi.org/10.3390/rs5063057

Li Y., Zhao X.Y., 2012. An empirical study of the impact of human activity on long-term temperature ch ange in China: A perspective from energy consumption. J. Geophys. Res. Atmos. 117, 17117. https://doi.org/10.1029/2012JD018132

Lindberg F., Grimmond C.S.B., Yogeswaran N., Kotthaus S., Allen L., 2013. Impact of city changes and weather on anthropogenic heat flux in Europe 1995–2015. Urban Clim. 4, 1–15. https://doi.org/10.1016/j.uclim.2013.03.002

Lu D.S., Tian H.Q., Zhou G.M., Ge H.L., 2008. Regional mapping of human settlements in southeastern China with multisensor remotely sensed data. Remote Sens. Environ. 112(9), 3668–3679. https://doi.org/10.1016/j.rse.2008.05.009

Lu Y., Wang Q.G., Zhang Y.Y., Sun P., Qian Y., 2015. An estimate of anthropogenic heat emissions in China. Int. J. Climatol. 36(3), 1134–1142. https://doi.org/10.1002/joc.4407

Wong M.S., Yang J.X., Nichol J., Weng Q.H., Menenti M., Chan P.W., 2015. Modeling of Anthropogenic Heat Flux Using HJ-1B Chinese Small Satellite Image: A Study of Heterogeneous Urbanized Areas in Hong Kong. IEEE Geosci. Remote Sens. Lett. 12(7), 1466–1470. https://doi.org/10.1109/LGRS.2015.2409111

Narumi D., Kondo A., Shimoda Y., 2009. Effects of anthropogenic heat release upon the urban climate in a Japanese megacity. Environ. Res. 109(4), 0–431. https://doi.org/10.1016/j.envres.2009.02.013

National Research Council. 2000. Cooperation in the Energy Futures of China and the United States. Washington, DC: The National Academies Press. https://doi.org/10.17226/9736

Nie W.S., Sun T., Ni G.H., 2014. Spatiotemporal characteristics of anthropogenic heat in an urban environment: A case study of Tsinghua Campus. Build. Environ. 82, 675–686. https://doi.org/10.1016/j.buildenv.2014.10.011

Nie W.S., Zaitchik B.F., Ni G.H., Sun T., 2017. Impacts of anthropogenic heat on summertime rainfall in Beijing. J. Hydrometeorol. 18(3) https://doi.org/10.1175/JHM-D-16-0173.1

Peng J., Chen S., Lü H.L., Liu Y.X., Wu J.S., 2016. Spatiotemporal patterns of remotely sensed PM 2.5, concentration in China from 1999 to 2011. Remote Sens. Environ. 174, 109–121. https://doi.org/10.1016/j.rse.2015.12.008

Sailor D.J., 2011. A review of methods for estimating anthropogenic heat and moisture emissions in the urban environment. Int. J. Climatol. 31(2), 189–199. https://doi.org/10.1002/joc.2106

Sailor D.J., Lu L., 2004. A top–down methodology for developing diurnal and seasonal anthropogenic heating profiles for urban area. Atmos. Environ. 38, 2737–2748. https://doi.org/10.1016/j.atmosenv.2004.01.034

Shi K.F., Chen Y., Yu B.L., Xu T.B., Yang C.S., Li L.Y., Huang C., Chen Z.Q., Liu R., Wu J.P., 2016. Detecting spatiotemporal dynamics of global electric power consumption using DMSP-OLS nighttime stable light data. Appl. Energy. 184, 450–463. https://doi.org/10.1016/j.apenergy.2016.10.032

Shi K.F., Yu B.L., Huang, Y.X., Hu Y.J., Yin B., Chen Z.Q., Chen L.J., Wu J.P., 2014. Evaluating the Ability of NPP-VIIRS Nighttime Light Data to Estimate the Gross Domestic Product and the Electric Power Consumption of China at Multiple Scales: A Comparison with DMSP-OLS Data. Remote Sens. 6, 1705–1724. https://doi.org/10.3390/rs6021705

Stewart I.D., Oke T.R., 2012. Local Climate Zones for Urban Temperature Studies. Bull. Amer. Meteorol. Soc. 93(12), 1879–1900. https://doi.org/10.1175/BAMS-D-11-00019.1

Sun R.H., Wang Y.N., Chen L.D., 2018. A distributed model for quantifying temporal-spatial patterns of

anthropogenic heat based on energy consumption. J. Cleaner Prod. 170, 601–609. https://doi.org/10.1016/j.jclepro.2017.09.153

Taha H., 1997. Urban climates and heat islands: albedo, evapotranspiration, and anthropogenic heat. Energy Build. 25(2), 99–103. https://doi.org/10.1016/S0378-7788(96)00999-1

Tomar V., Mandal V.P., Srivastava P., Patairiya S., Singh K., Ravisankar N., Subash N., Kumar P., 2014. Rice Equivalent Crop Yield Assessment Using MODIS Sensors' Based MOD13A1-NDVI Data. IEEE Sens. J. 14(14), 3599–3605. https://doi.org/10.1109/JSEN.2014.2329185

Wang F.T., 2002. Advances in climate warming impact research in China in recent ten years. Q. J. Appl. Meteorol. Sci. 13(6), 755–766. (in Chinese)

Wang Y., Chen T., Sun R., 2016. Assessing the spatiotemporal characteristics of anthropogenic heat in Beijing. China Environ. Sci. 36(7), 2178–2185. (in Chinese)

Wong D.W.S., 1999. Several Fundamentals in Implementing Spatial Statistics in GIS: Using Centrographic Measures as Examples. Geog. Inf. Sci. 5(2), 163–174. https://doi.org/10.1080/10824009909480525

Xie M., Liao J.B., Wang T.J., Zhu K.G., Zhuang B.L., Han Y., Li M.M., Li S., 2016. Modeling of the anthropogenic heat flux and its effect on regional, meteorology and air quality over the Yangtze River Delta region, China. Atmos. Chem. Phys. Discuss. 15(22), 32367–32412. https://doi.org/10.5194/acp-16-6071-2016

Yang W.M., Luan Y.B., Liu X.L., Miao L.J., Cui X.F., 2017. A new global anthropogenic heat estimation based on high-resolution nighttime light data. Sci. Data. 4:170116. https://doi.org/10.6084/m9.figshare.c.3647903.v1

Yang X., Wang S.J., Zhang W.Z., Zhan D.S. Li J.M., 2016. The impact of anthropogenic emissions and meteorological conditions on the spatial variation of ambient SO2 concentrations: A panel study of 113 Chinese cities. Sci. Total Environ. 318, 584–585. https://doi.org/10.1016/j.scitotenv.2016.12.145

Zhang Q.L., Schaaf C., Seto K.C., 2013. The Vegetation Adjusted NTL Urban Index: A new approach to

reduce saturation and increase variation in nighttime luminosity. Remote Sens. Environ. 129(2), 32–41. https://doi.org/10.1016/j.rse.2012.10.022

Zhou Y., Ma T., Zhou C., Xu T., 2015. Nighttime Light Derived Assessment of Regional Inequality of Socioeconomic Development in China. Remote Sens. 7, 1242–1262. https://doi.org/10.3390/rs70201242

Zhao Y., Lu J., 2011. The investigation of anthropogenic heat emission of building group. Refrig. Air Conditioning. 25 sup., 239–244. https://doi.org/10.3969/j.issn.1671-6612.2011.z1.059

Zhou Y.Y, Weng Q.H., Gurney K. R., Shuai Y.M., Hu X.F., 2012. Estimation of the relationship between remotely sensed anthropogenic heat discharge and building energy use. ISPRS-J. Photogramm. Remote Sens. 67, 65–72. https://doi.org/10.1016/j.isprsjprs.2011.10.007

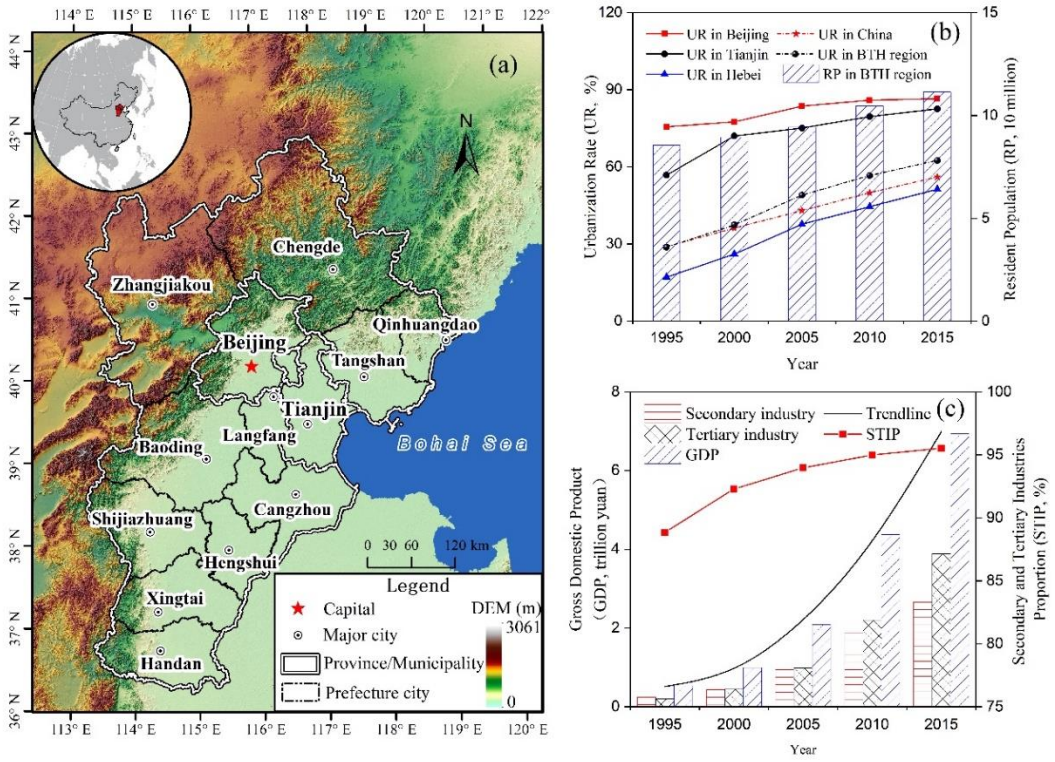

553

554 **Fig. 1.** Spatial distribution and urbanization of study area (a) Location of Beijing-Tianjin-Hebei region (BTH

555 region) in China; (b) Urbanization rate (UR) and resident population (RP) from 1995 to 2015; (c) Gross district

556 product (GDP) and secondary and tertiary industries proportion (STIP) from 1995 to 2015.

557

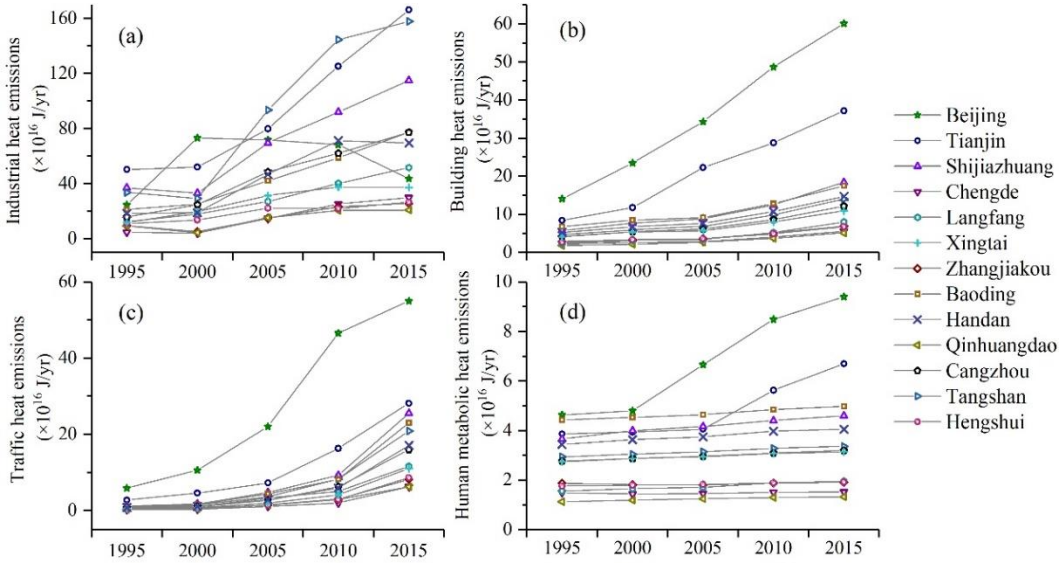

558

559 **Fig. 2.** Anthropogenic heat emissions from different sources of the cities/municipalities in BTH region from 1995 to

560 2015. (a) Industrial heat emissions; (b) Building heat emissions; (c) Traffic heat emissions; (d) Human metabolic heat

561 emissions

562

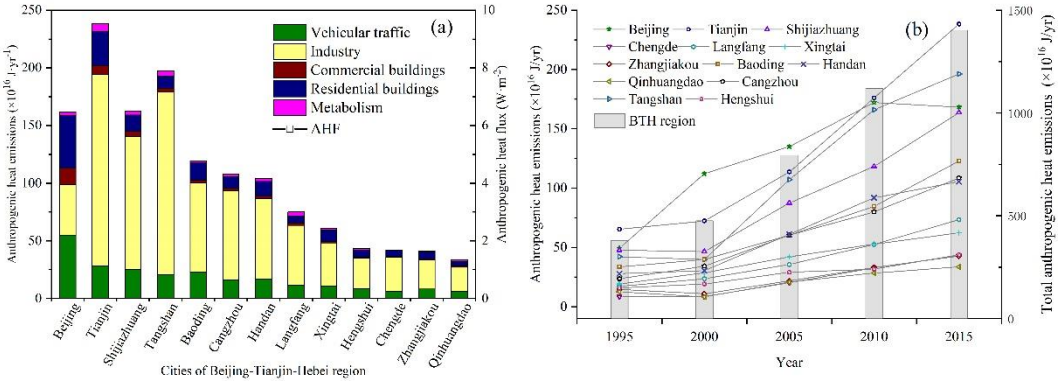

563

564 **Fig. 3.** Anthropogenic heat emissions and anthropogenic heat flux (AHF) of different sources in 2015 and the

565 anthropogenic heat emissions between 1995 and 2015 in the cities of Beijing-Tianjin-Hebei region

566

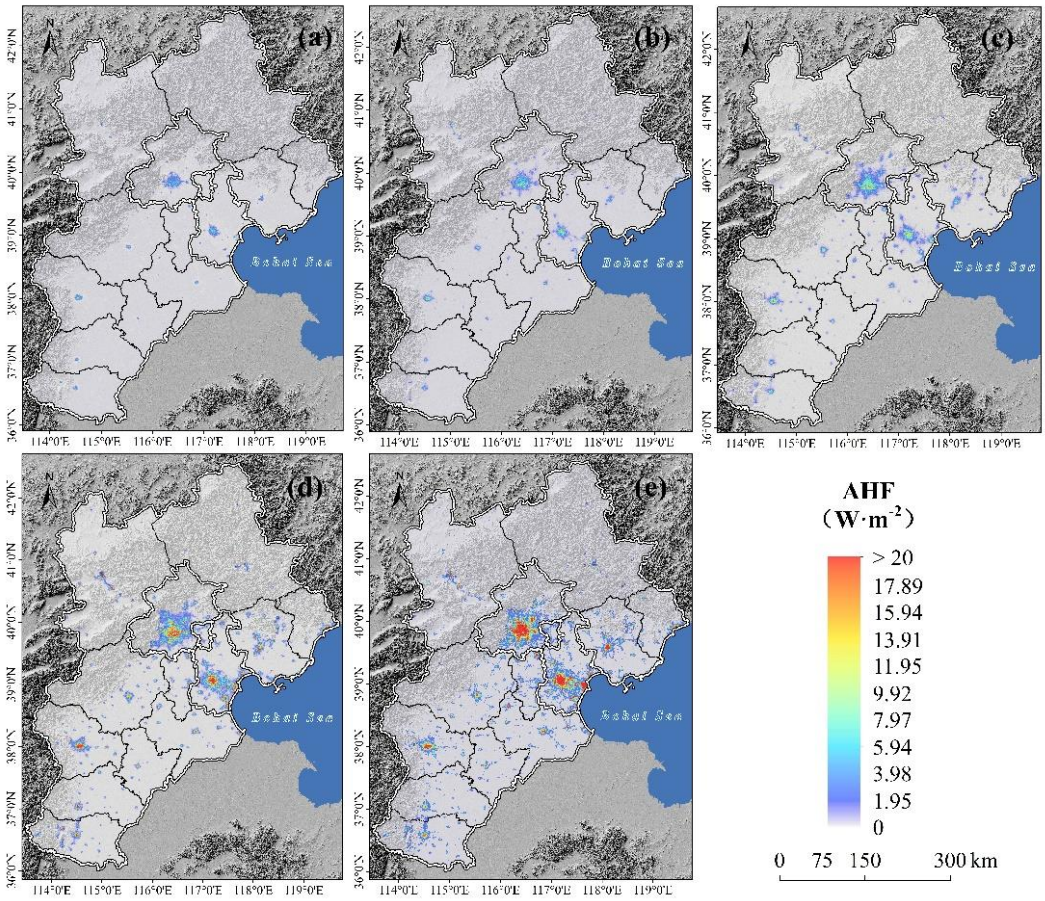

567

568 **Fig. 4.** The pixel-based anthropogenic heat flux (AHF) results between 1995 and 2015 in Beijing-Tianjin-Hebei

region. (a) 1995; (b) 2000; (c) 2005; (d) 2010; (e) 2015

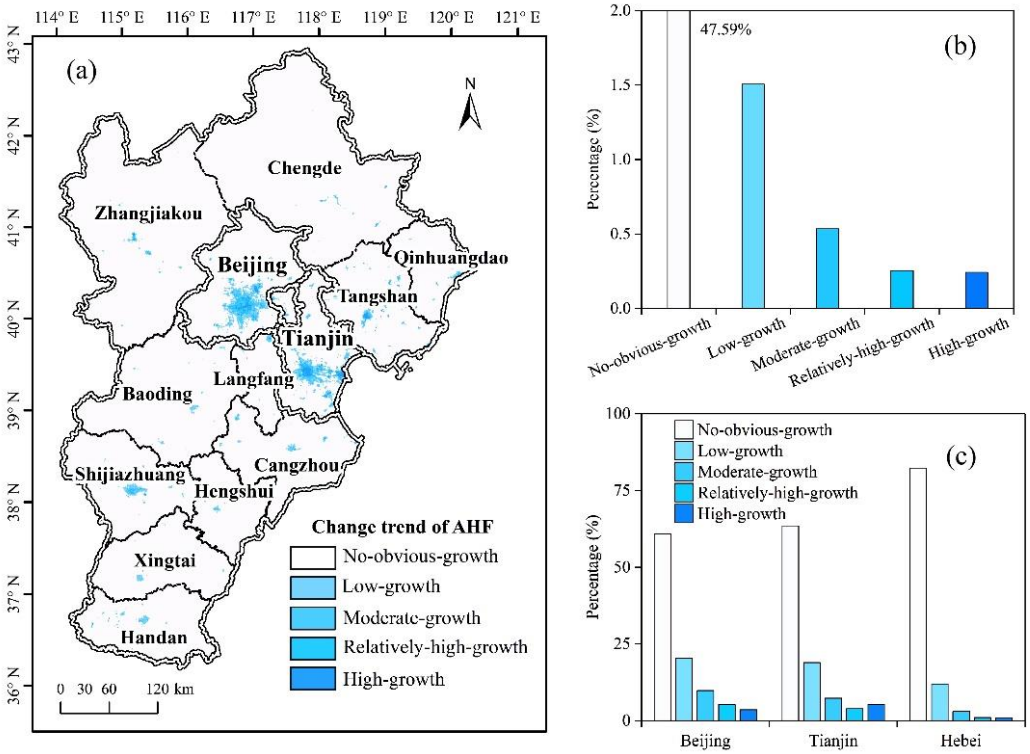

Fig. 5. Spatial distribution of anthropogenic heat flux (AHF) change and areal percentage of each AHF growth type between 1995 and 2015. (a) Change trend of AHF in Beijing-Tianjin-Hebei (BTH) region; (b) Areal percentage of no-obvious-growth, low-growth, moderate-growth, relatively-high-growth, and high-growth AHF in BTH region; (c) Areal percentage of 5 types of AHF growth in Beijing, Tianjin and Hebei.

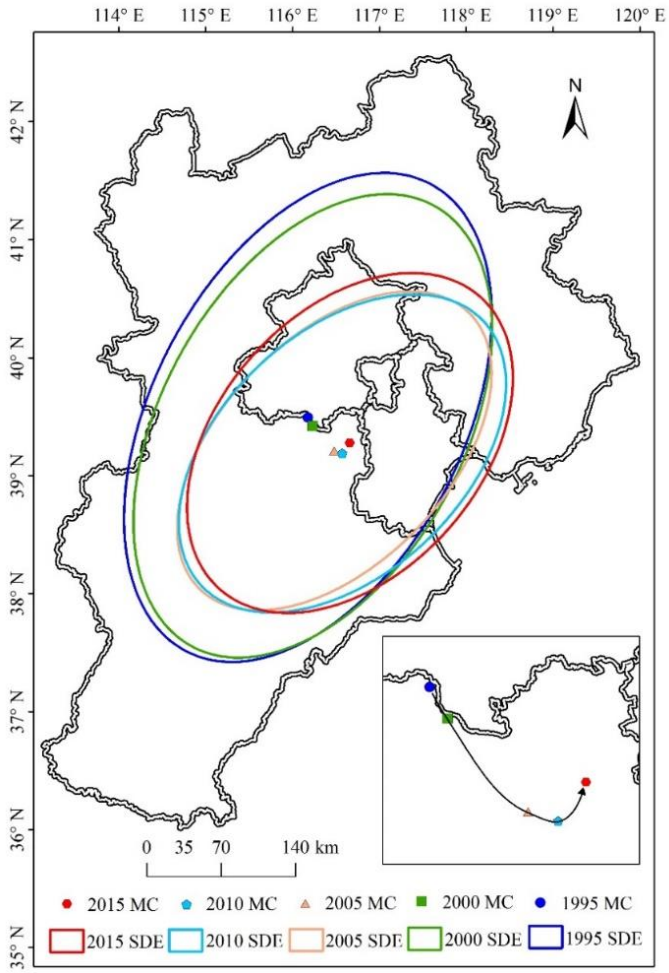

577

578 **Fig. 6.** Spatial changes in the mass center (MC) and standard deviational ellipse (SDE) of anthropogenic heat flux

579 in Beijing-Tianjin-Hebei region between 1995 and 2015. See text for index definitions.